UCRL-JC-126351
PREPRINT

Strong Ground Motion Synthesis along the Sanyi-Tungshih-Puli Seismic Zone using Empirical Green's Functions

L. Hutchings
F.T. Wu
R.-J. Rau
S. Jarpe
P. Kasameyer
W. Foxall

This paper was prepared for submittal to the
1997 Central Weather Bureau 100th Anniversary International Conference on Weather Analysis and Forecasting
Taipei, Taiwan
March 3-5, 1997

January 1997

Lawrence Livermore National Laboratory

Work performed under the auspices of the U.S. Department of Energy by Lawrence Livermore National Laboratory under Contract W-7405-ENG-48.

Strong Ground Motion Synthesis along the Sanyi-Tungshih-Puli seismic zone using Empirical Green's functions

International Conference on Weather Analysis and Forecasting, March 3-5,1997

Lawrence Hutchings[1]; Francis T. Wu[2]; Ruey-Juin Rau[3]; Steve Jarpe[4]; Paul Kasameyer[1]; and William Foxall[1]

1) Lawrence Livermore National Laboratory, P.O. Box 808, Livermore Ca. 94551, USA; telephone (510) 423-0354, fax: (510) 422-3925, email: hutchings2@llnl.gov
2) Department of Geological Sciences, State University of New York, Binghamton, New York, 13902-6000, USA; telephone: (607)777-2512; fax: (607)777-2288; email: wu@sunquakes.geol.binghamton.edu
3) Institute of Earth Sciences, Academia Sinica,Nankang P.O. Box 1-55, Taipei, Taiwan. rau@earth.sinica.edu.tw
4) Institute for Crustal Studies, University of California, Santa Barbara, California 93106-9630, USA; telephone: (520) 775-6803; email: jarpe@computerlink.com.

Abstract

We synthesize strong ground motion from a M=7.25 earthquake along the NW-trending Sanyi-Tungshih-Puli seismic zone. This trend extends from Houlong to Taichung and forms a nearly continuous 78 km long seismic zone identified by the occurrence of M<5 events. It extends from shallow depth all the way down to about 40 km. The entire length of the fault, if activated at one time, can lead to an event comparable to that of the 1995 Kobe earthquake. With the improved digital CWBSN data now provided routinely by CWBSN, it becomes possible to use these data as empirical Green's functions to synthesize potential ground motion for future large earthquakes. We developed a suite of 100 rupture scenarios for the earthquake and computed the commensurate strong ground motion time histories. We synthesized strong ground motion with physics-based solutions of earthquake rupture and applied physical bounds on rupture parameters. The synthesized ground motions obtained are source and site specific. By having a suite of rupture scenarios of hazardous earthquakes for a fixed magnitude and identifying the hazard to a site from the statistical distribution of engineering parameters, we have introduced a probabilistic component to the deterministic hazard calculation. The time histories suggested for engineering design are the ones that most closely match either the average or one standard deviation absolute acceleration response values.

Introduction

Realistic time histories should be used to reduce uncertainties in estimation of standard engineering parameters (Hutchings, 1991) and for nonlinear dynamic analysis of structures (McCallen and Hutchings, 1996). Here we present a methodology for developing realistic synthetic strong ground motions for specific sites from specific faults. We hypothesized a M=7.25 earthquake (moment magnitude, Hanks and Kanamori, 1979) that ruptures 78 km along the Sanyi-Tungshih-Puli (Houlong to Taichung) seismic zone (Rau and Wu, 1995) as an example of a design earthquake calculation. The length of the fault, if activated at one time, can lead to an event comparable to that of the 1995 Kobe earthquake. Several historical events occurred near or in the seismic zone: M= 6.5 in 1916; M= 6.0 in 1916; and, M=6.1 in 1917. The locations of these events have relatively large uncertainties. Also, the M=7.1 Hsinchu-Taichung earthquake occurred approximately at 24.39N, 120.68E in 1935. We synthesize strong ground motion at NSY (TCU128; 24.416N 120.761E).

Realistic time histories should include the effects of geologic conditions along the propagation path from the fault and at the site itself. Geologic conditions can significantly alter the amplitudes of seismic energy, and can cause focusing and scattering of energy. Also, at sites close to large faults it is critical to account for the effects of finite fault rupture. These include seismic arrivals radiated from portions of the fault that can be tens of kilometers apart and arrive at the same time, and directivity effects that can significantly enhance or diminish amplitudes of the wave field. In addition, the superposition of direct and scattered body-waves and surface-waves will result in an extremely complicated wavefield and should be modeled. To model all these affects we synthesize strong ground motion with physics based solutions of earthquake rupture that utilize empirical Green's functions and apply physically based rupture parameters. We have developed an exact solution to the representation relation for finite rupture that utilizes either empirical or synthetic Green's functions (Hutchings and Wu, 1990; Hutchings, 1991; Jarpe and Kasameyer, 1996). Here, we use recordings of small earthquakes to provide empirical Green's functions for frequencies 5.0 to 25.0 Hz, and analytical calculations to provide synthetic Green's functions for frequencies 0.05 to 5.0 Hz. We synthesize the entire wavetrain and for three components. Site soil can also significantly affect ground motions with non-linear effects, but here we only present linear ground motions that might be expected at a rock outcrop.

The synthesis approach uses empirical Green's functions solely to obtain the Green's functions of the representation relation, thereby allowing for completely synthetic rupture models (Wu, 1978; Hutchings and Wu, 1990). Thus, no *a priori* assumptions are imposed on the rupture process, and a suite of kinematic rupture models can be used. Most empirical Green's functions synthesis approaches model fault rupture as a composite of smaller earthquakes, which have a multitude of small events rupturing independently over the fault surface (Hartzell, 1978; Hadley and Helmberger, 1980; Irikura, 1983; Papageorgiou and Aki, 1983; Munguia and Brune, 1984; Joyner and Boore, 1986; Boatwright, 1988; Wennerberg, 1990; and, Aki and Irikura, 1991). There is little physical or empirical basis for composite models of earthquakes. Also, composite models of faulting rely on scaling relations of earthquakes to determine the number of small earthquakes necessary to synthesize a large earthquake, and have a difficulty in matching the low and high frequency of synthesized seismograms to observed records (Joyner and Boore, 1986; Boatwright, 1988; Tumarkin *et. al.,* 1994; Frankel 1995). Our modeling approach only requires that the number of small earthquakes used in the synthesis is such that the sum of their moments add up to the moment of the large earthquake, which matches the low frequency of observed seismograms. The high frequency is matched simply by using appropriate rupture parameters (Hutchings, 1994).

With the improved digital CWBSN data now provided routinely by CWBSN it becomes possible to use this data as empirical Green's functions to synthesize potential ground motion for future large earthquakes. Figure 1 shows the location of the hypothesized fault, station location, and location of events used to obtain empirical Green's functions. The rock under NSY is mostly Pleistocene gravel (85%) mixed with mud or sand (15%) which is not well cemented. This gravel can be as thick as 2000 m. The geology beneath the site is such that it may respond non-linearly during strong shaking. If that is true, the results of this study would have to be deconvolved to a bedrock ground motion and the response of the soil layer included in an upward propagation of the seismic energy.

We model the rupture process as a continuous rupture over fault segments with variable slip amplitude. Areas of high slip are called asperities. This model is consistent, within the frequency range of resolution, with inversion studies (Wald et. al., 1990, 19091, 1993, 1995; Beroza and Spudich, 1988; Hartzell and Heaton, 1988; Hartzell 1989) and with what is known from dynamic rupture models about how earthquakes rupture (Rice and Ruina, 1983; Kostrov and Das, 1988). However, these studies only resolve fault slip histories up to spatial resolutions of a couple of kilometers and frequencies up to one hertz. Nevertheless, our method provides good fits to observed seismograms up to 25 Hz when these models are used. The complexity added to rupture by many ground motion synthesis approaches is not necessary to synthesize observed seismograms, and there is no evidence that earthquakes rupture is highly complex at short spatial or temporal dimensions.

We developed a suite of 100 rupture scenarios for the hypothesized M=7.25 earthquake on the Sanyi-Tungshih-Puli fault and computed the commensurate strong ground motion time histories.The scenarios were developed by randomly varying rupture parameters within a range of physical limits obtained from independent research. This approach is useful if the range of possible fault rupture histories is narrow enough to functionally constrain the range of strong ground-motion predictions. This is tested in this study. Log-normal average and one standard deviation values of peak acceleration, pseudo-velocity response, and absolute acceleration response spectra were derived from the suite of synthesized strong ground motion. The time history used for rock outcrop motion is the time history that most closely matches the one standard deviation values. By having a suite of rupture scenarios of hazardous earthquakes for a fixed magnitude and identifying the hazard to the site from the one standard deviation value of engineering parameters, we have introduced a probabilistic component to the deterministic hazard calculation.

Green's Functions

The basic premise in synthesizing with empirical and synthetic Green's function is that each offers the best accuracy over particular frequency bands. Empirical Green's functions are defined here as recordings of effectively impulsive point source events (Hutchings and Wu, 1990). The empirical Green's functions have a better accuracy at high frequencies, where geologic inhomogeneities are not well modeled, and the synthetic Green's functions have better accuracy at lower frequencies, where empirical Green's functions do not have sufficient energy. The overlap in this study is in the range from $3 \le f \le 5$ Hz, where the geology can be modeled with some accuracy and the empirical Green's function have sufficient energy to be well recorded.

We computed synthetic Green's functions using the reflectivity code of Kennett (1983). This solution extends to D.C., but does not include near-field terms. Focal mechanism radiation pattern is used for synthetic Green's

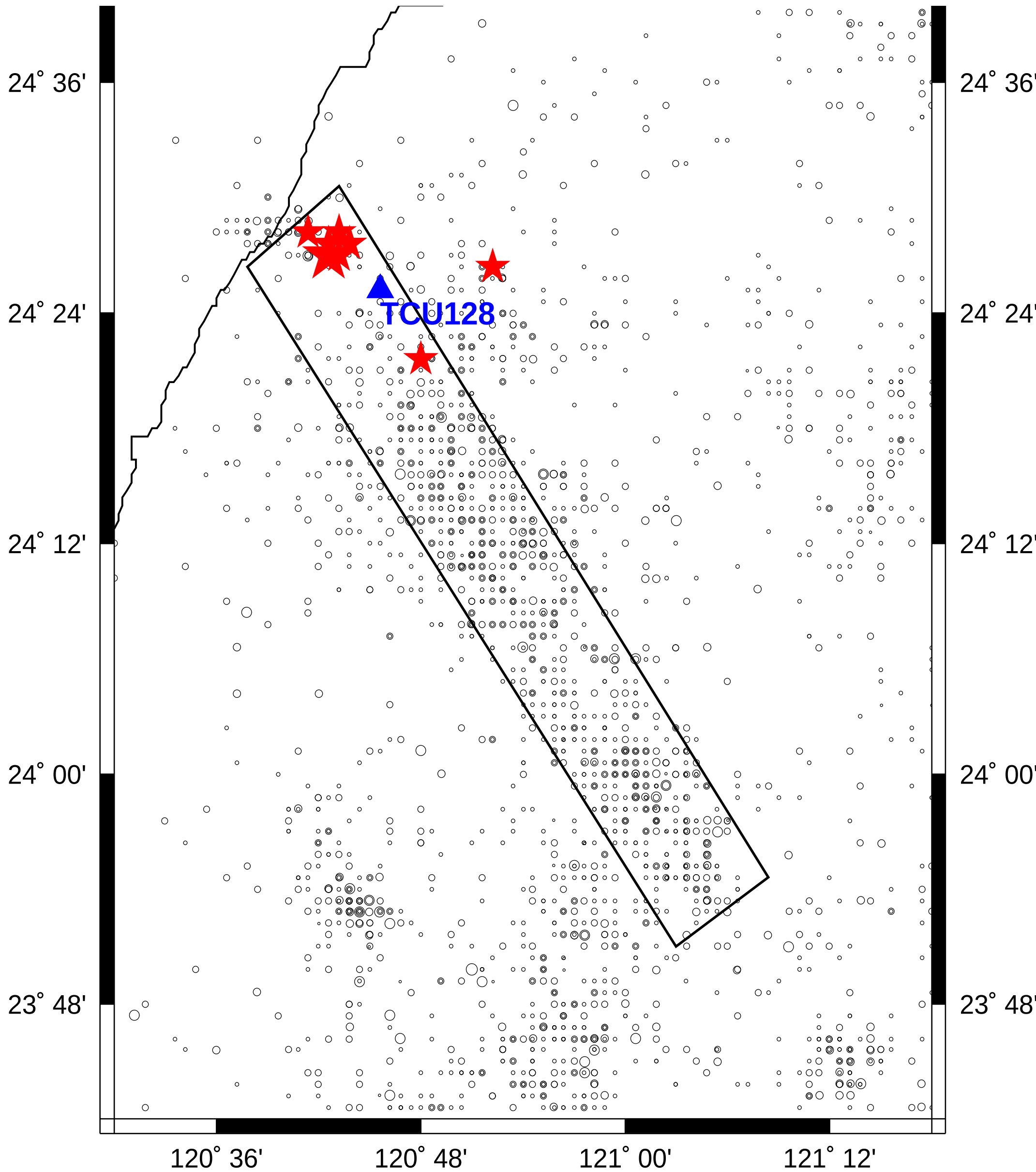

Figure 1. Seismicity in northwestern Taiwan. The box outlines the surface projection of the Sanyi-Tungshih-Puli seismic zone and hypothesized area of fault rupture for a M=7.25 earthquake. The stars indicate locations of events used to obtain empirical Green's functions, and TCU128 is the station location (NSY).

functions solutions to the finite rupture. We only considered solutions for frequencies greater than 0.05 Hz (20 sec period), as lack of near-field arrivals diminish the reliability of solutions for frequencies lower than this. A one dimensional velocity model was used for the calculations.

Empirical Green's functions should be recorded at the site of interest and from source events along the faults of interest, since site response and near source propagation path effects are highly variable. Empirical Green's functions include the actual effects of velocity structure, attenuation, and geometrical spreading. However, it is not possible to record empirical Green's functions from all locations along a fault of interest and with the same focal mechanism solution, so that source locations of empirical Green's functions have also been interpolated to fill in the fault. Figure 1 shows epicenter locations of source events used for empirical Green's functions. The limited locations of events that provide empirical Green's functions means that the site response is primarily captured by the empirical Green's functions, and that propagation path effects from locations to the south of the site area are not captureed.The spatial dependence of empirical Green's functions has been researched by Hutchings and Wu (1990) and they found that the variability in ground motion due to differences in source location and/or focal mechanism solutions are much less than that due to the site response, and Hutchings (1991), Hutchings (1994), and Jarpe and Kasameyer (1996) found that interpolation for different source locations along a fault works quite well. Also, it is not necessary to have source events fall directly along the fault of interest, but to be located near the fault. In synthesis, we have the option of correcting for different focal mechanism solutions, but Hutchings and Wu (1990) and Jarpe and Kasameyer (1996) found that for high frequencies it does not improve the synthesis. Interpolation is performed by correcting for attenuation, 1/R, and P- and S-wave arrival times due to differences in source distance. We include the radiation pattern effect for low frequencies, when we use synthetic Green's functions.

Sanyi-Tungshih-Puli Fault Model

The NW-SE-trending seismic zone in the shallow crust of the mountains of central Taiwan, called the "Sanyi-Tungshih-Puli Seismic Zone" (Lee et al., 1996), is modeled here as capable of a magnitude 7.25 earthquake. The zone forms a nearly continuous 78 km long seismic zone identified by the occurrence of magnitude less than M=5 events. It extends from shallow depth all the way down to about 40 km (Rau and Wu, 1995). There are two inclined seismic layers along this seismic zone. Figure 2 shows a cross section across the center of the seismic zone. It is evident that there are two dipping bands of seismicity that are interpreted here as two distinctive faults. So, although we may assume the large earthquake can occur along the shallow dipping plane, the seismicity in the deeper layer may present an additional seismic hazard. **T**he shallow zone extends from 7 to 14.5 km deep and dips at 30^{o}E (Rau and Wu, 1995). This is the zone for which we model a possible earthquake hazard. The deeper zone of activity the extends from 20 to 40 km depth. We do not model an earthquake that may occur in this zone. The fault is modeled here to extend from 5 to 16 km depth; the extended portion of rupture is expected due to overshoot for a large earthquake. Figure 1 shows the surface projection of the modeled fault. Wu et. al. (1996) show that this portion of Taiwan is under con-

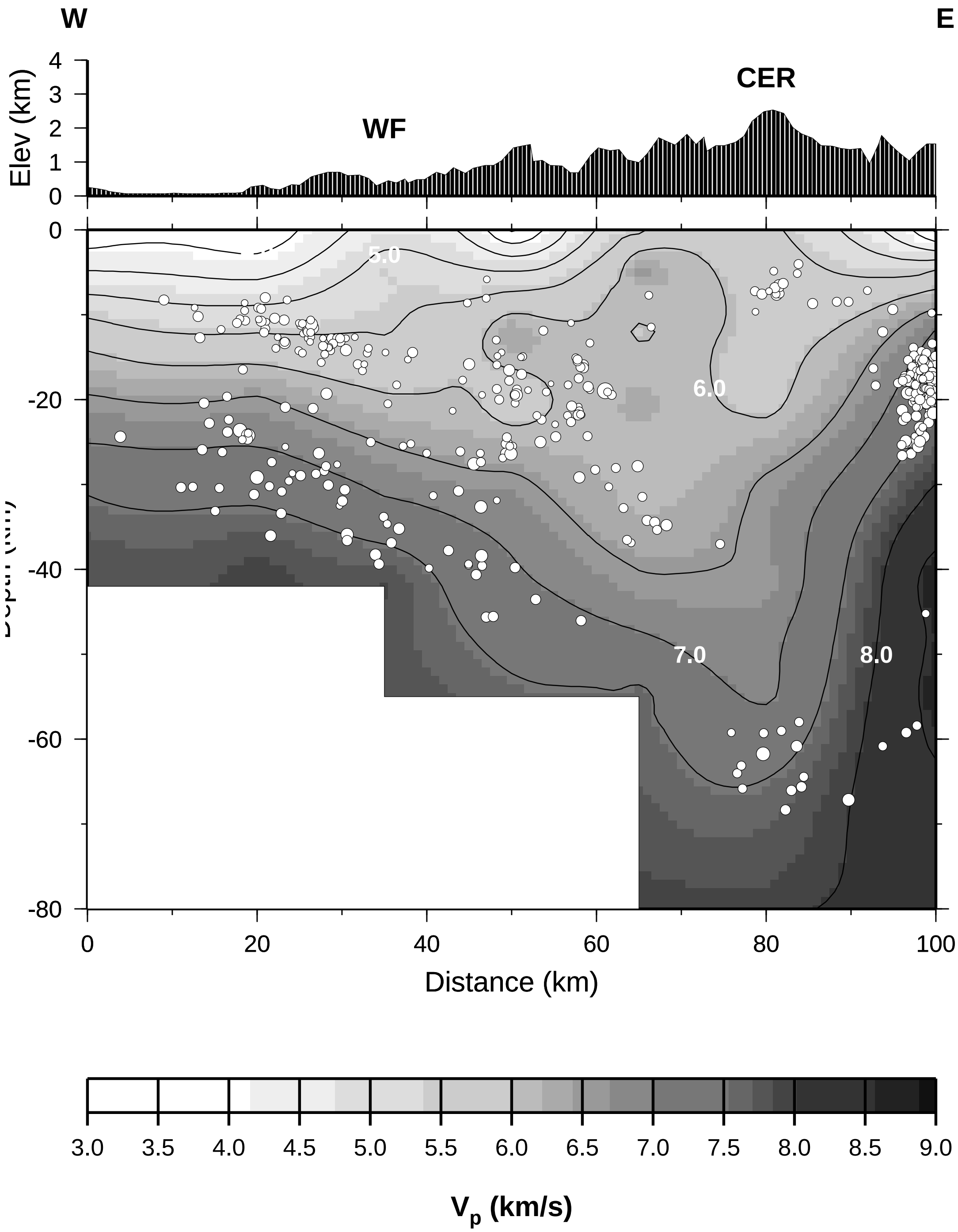

Figure 2. A cross section of seismicity across the Sanyi-Tungshih-Puli seismic zone (from Rau and Wu, 1995). The upper band of seismicity extends to about 20 km depth, and the lower band extend to about 60 km depth. Fault rupture is modeled for the upper band of seismicity.

vergence due to the collision of the Philippine plate with the Ureas continent. However, the oblique motion of the convergence suggests that a portion of strike slip motion may also be expected. Also, the Taiwan Oil Company geologists (Hsu et al., 1996) indicate that this seismic zone may have a sinistral strike-slip fault motion "Puli fault" associated with it. Therefore, the fault is modeled here as a blind thrust fault with equal portions of reverse and right-lateral strike slip motion. The upper edge of the fault is at 5 km depth, extends between 23.83N, 121.02E and 24.42N, 120.59E with a length of 78 km, has and a strike of N327^{o}E, dips 30^{o}E, and it has a width of 18 km.

Synthetic Rupture Models

Our earthquake rupture models rely on moment, fault geometry, hypocenter, rupture roughness, rupture velocity, healing velocity, slip vector, and asperity location. Moment and fault geometry (extent of rupture and its orientation) are held fixed, while the other parameters were allowed to vary within limits. The fault rupture surface area was discretized into 0.01 Km^2 elemental areas, which are small enough that modeled rupture is continuous for frequencies $f \le 25.0$ Hz. The rupture initiates at the hypocenter and propagates radially at some fraction of the shear wave velocity. We used the Kostrov slip function to calculate the slip at a point; we approximated the shape as a ramp. We arbitrarily limited the rupture propagation factor in the Kostrov slip function to be equal to or less than the rupture time to the closest fault edge from the hypocenter. We used a computer program that randomly varies independent rupture parameters subject to the following constraints. Other parameters are either fixed or calculated from the rupture model.:

ASPERITIES are included to add high slip amplitudes to portions of the rupture. Asperities are circular and have a diameter randomly chosen to be between 0.2 and 0.8 times the fault width. The number of asperities is randomly selected for each scenario. Stress drop in asperity portions of rupture are higher than elsewhere.

ROUGHNESS is simulated as elements resisting rupture, then breaking. A percentage of elements (0, 10, 20, 33, or 50%) have a shortened rise times 10-90% those of neighboring elements, but with rupture completed at the same time as neighboring elements. These “rough” elements have corresponding high stress drop.

MOMENT is constrained to be 8.0x10^{26} dyne-cm for the total rupture, including asperities. However, the moment of asperities is randomly selected, subject to the constraint that the maximum displacement is 5-10m. Rigidity (proportional to shear wave velocity, except near the surface) diminishes near the surface so that the moment contribution diminishes. However, stress drop is also modeled to diminish (discussed below), so significant displacement can occur near the surface, although not seismogenic.

HYPOCENTER was constrained to occur at least 1 km from the fault ends, 2 km from the lower limit of the fault, and at depth greater than 7.5km. The limit at the lower portion of the fault is because of the weakening in rigidity as the aseismic zone is approached, and the limit to greater than 7.5 km is due to the observation that past earthquakes originate at depth.

RUPTURE VELOCITY is randomly selected to be from 0.75 to 1.0 times the shear wave velocity.

HEALING VELOCITY is the velocity for the stress pulse that terminates slip. The healing phase is initiated after the rupture arrives at any fault edge. The free surface is not allowed to be a healing boundary for rupture, because significant seismic pulses that are necessary to shut down slip are not generated from the surface (Das and Kostrov, 1985; Scholz, 1990). The healing velocity is randomly selected to be between 0.8 and 1.2 times the rupture velocity, which is between the Rayleigh and shear wave velocities.

RISE TIME is equal to the time it takes, after the initiation of rupture, for the first healing phase to arrive.

STRESS DROP is a dependent variable derived from the Kostrov slip function and allowed to vary due to three effects modeled in rupture. Asperities and rough rupture are allowed to have a different stress drop than surrounding portions of the fault rupture (discussed above). Also, stress drop is constrained to diminish near the surface of the earth at the rate of 10 + 0.75 x the confining pressure due to the lithostatic load (300 bars at 1.7 km depth). The minimum of the stress drop calculated using this constraint and the full rupture stress drop is used.

SLIP VECTOR is constrained to 135^{o} for equal portions of reverse and right-lateral strike slip fault motion.

Prediction Uncertainty

In the terminology of Abrahamson et al.,1990), our prediction uncertainty has two elements: 1) parametric uncertainty, which arises from uncertainty as to which scenario will occur, and (2) modeling and random errors caused by not modeling the actual rupture process correctly and by factors such as uncertainties in moment estimates for empirical Green's functions and errors caused by interpolation of source events along the fault surface.

We estimated the parametric uncertainty by generating a suite of time histories from 100 sets of independent parameters. We selected these sets at random by assuming that the parameters are uncorrelated and that each is uniformly distributed through its allowed range. Figure 3 shows the average (in log space) of the absolute acceleration response (AAR) spectra for the two horizontal components calculated for each of the 100 parameter sets. All these parameter sets represent earthquakes with the same moment and fault rupture area, parameters that might be successfully anticipated in advance. As Figure 3 shows, a broad range of possible response spectra could be generated from an event whose moment and fault rupture area are fixed.

Jarpe and Kasameyer (1996) estimated the second element of uncertainty, modeling and random errors, by comparing computed and observed records for the 1989 Loma Prieta earthquake, whose independent parameters were well determined. This error is unknown for the site at NSY, but is assumed to be equal to the one standard deviation value obtained by Jarpe and Kasameyer (1996). The total source uncertainty is characterized by adding the parametric and "random plus modeling" standard deviation estimates (0.80 and 0.55 at 1 Hz) in quadrature. The mean and 84th percentiles of the AAR distribution calculated in this manner are given by the dark line in Figure 4. The average peak acceleration is 0.62g, and the plus one standard deviation value is 1.33g.

We examine the AAR data at a single frequency (1Hz) to illustrate how the parametric error can be estimated and how that estimate is improved by calculating more scenarios. Figure 5 is a histogram of the natural logarithms of the calculated values at that frequency. The data are distributed normally in log-space with a sample mean and standard deviation of -2.85

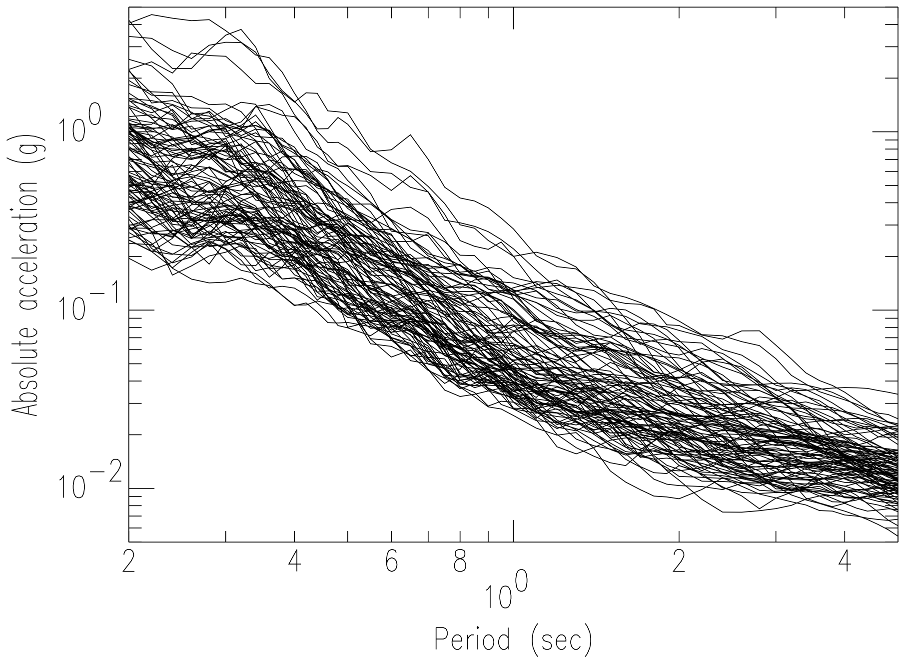

Figure 3. The AAR response curves for the 100 scenarios.

and 0.53, and they pass a χ^2 test (Freund, 1962) for the log normal distribution. Figure 6 shows the evolution of the sample mean as a function of the number of scenarios run. The uncertainty in the mean is estimated from the observed variability and number of points used, approximating the data-distribution as log-normal. A similar calculation was made for the “84th percentile” represented by the sum of the sample mean and sample standard deviation. The uncertainty in the sum is estimated by assuming the errors in the mean and standard deviation are independent (Hald, 1952). Estimates of the mean and 84th percentile vary significantly with the number of scenarios, but the final estimates (for 100 scenarios) always lie within the 1σ bounds for the estimate uncertainty, suggesting that the approximate error model gives a useful estimate of the uncertainty. The uncertainties decrease significantly as more scenarios are added. The uncertainty in the natural logarithm of the mean decreased from 0.14 after 10 scenarios, to 0.05 (corresponding to approximately 0.003g) after 100. The bounds for the 84th percentile are about $\pm$.01g after 100 runs.

Hazard

A methodology for identifying the ground motion hazard to a site is to choose an acceptable probability from the suite of hazards from the 100 scenarios. If either the mean or $+1\sigma$ AAR (50th or 84th percentile) is chosen to identify the hazard, then time histories with AAR near these values would represent the hazard. It is not recommended to modify AAR to match a “target” spectrum, because this would effectively alter the rupture scenario and may inadvertently generate a non-physical model. Further, in non-linear structural analysis more than one time history should be selected. Rupture models TAI01 and TAI33 generated time histories that had AAR closest to the mean and $+1\sigma$, respectively. Figure 7

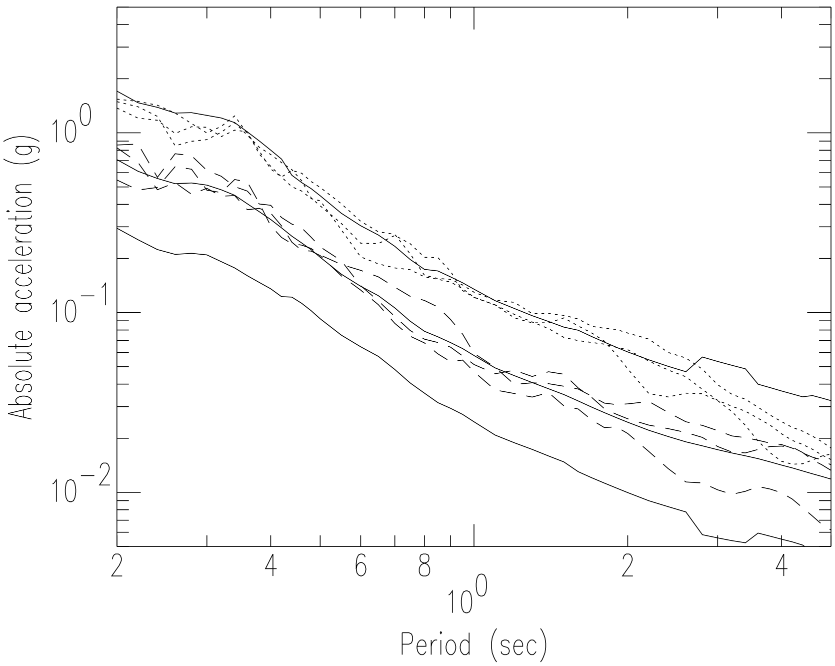

Figure 4. Mean and one standard deviation values of AAR (solid), and AAR values for the three scenarios that match the mean and plus one standard deviation (dashed)

shows the slip distribution and hypocenter for these models. Figure 8 shows the time histories; the top three are the three components of acceleration, the middle three are the same records integrated to displacement, and the bottom three are the displacement values. This time history accelerogram is for frequencies 0.01 to 25.0 Hz. The solution from 5.0 to 25.0 Hz was obtained from a synthesis using empirical Green's functions.

Discussion

The hazard for a possible M=7.25 earthquake along the Sanyi-Tungshih-Puli seismic zone was predicted at site NSY. The work presented here is a demonstration of a methodology to predict a range of ground motion hazard. This allows for a probabilistic component in selecting the hazard for engineering design purposes. From Figure 8, the model that most closely matches the mean hazard (TAI01) shows peak accelerations near 0.5g and durations greater than 20 seconds. Figure 7 shows that this ground motion is due to a fairly smooth rupture model that does not include asperities. The model that most closely matches the one standard deviation value (TAI33) has peak accelerations near 1.5g and durations that are similar to those of the mean model. From Figure 7, it is apparent that the higher peak accelerations are due to the location of asperities.

The methodology presented provides a means to model all the physical effects of finite fault rupture. The velocity records show a long period "fling" due to fault-normal directivity effects. Since station NSY is located directly above a portion of the fault, one would also

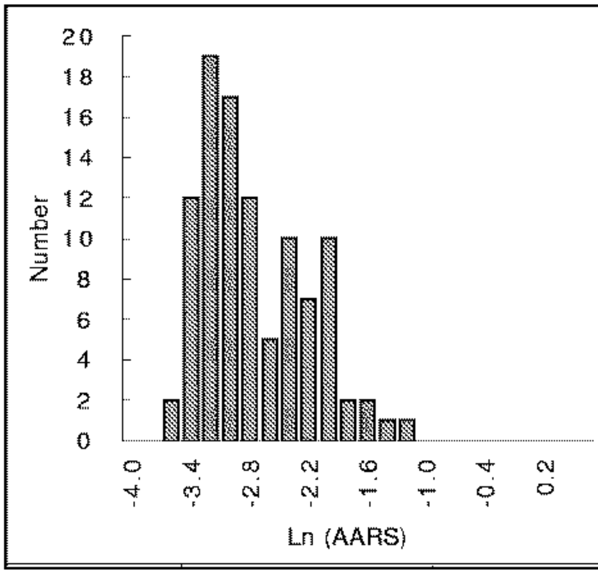

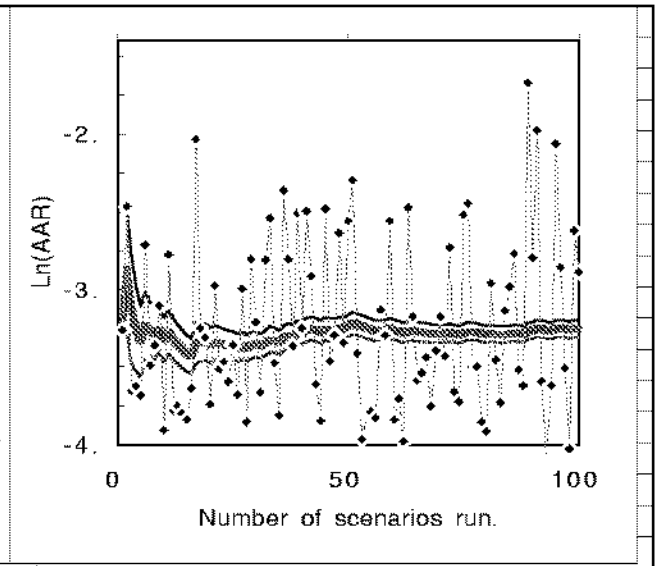

Figure 5. Histograms of number of scenarios as a function of AAR at 1.0 second period

Figure 6. Estimation of the mean (dark line) AAR at 1.0 s, its uncertainty, and the individual AAR values.

expect a static offset left after the earthquake. This is evident in Figure 7 displacement plots (although, model TAI33 has some drift that is an artifact).

Empirical Green's functions provided a means to constrain the uncertainties due to geologic inhomogeneities. However, the sensitivity of the instrumentation was such that only fairly large earthquakes (M>3.0) located nearby were recorded, and could provide empirical Green's functions. To improve constraints on geological effects at greater distances, lower gain settings would have to be applied. Also, the instrumentation noise level was such that frequencies below about 5.0 Hz were not well recorded. This necessitated using synthetic Green's functions for frequencies higher than their expected reliability.

Future applications of the methodology in Taiwan could greatly reduce uncertainties in prediction of strong ground motion for potential large earthquakes.

References

Abrahamson, N. A., P. G. Somerville, and C. A. Cornell (1990), *Uncertainty in Numerical Strong Motion Predictions*, in *Proc. 4th U.S. National Conf. Earthquake Engineering*, Vol. 1 (Earthquake Engineering Research Institute, 20–24 May, Palm Springs, California).

Aki, K., and K. Irikura (1991). Characterization and mapping of earthquake shaking for seismic zonation, in *Proceedings of the Fourth International Conference on Seismic Zonation, Vol. I*, EERI, Oakland, 61-110.

Beroza, G.C. and P. Spudich (1988) Linearized inversion for fault rupture behavior: application to the 1984 Morgan Hill, California earthquake. *J. Geophys. Res.* **93** 6275-6296.

Boatwright, J. (1988). The seismic radiation from composite models of faulting, *Bul. Seis. Soc. Am.* **78**, 489–508.

Das, S., and B. V. Kostrov (1985), *An Elliptical Asperity in Shear: Fracture Process and Seismic Radiation*, Geophys. J. Roy. Astron. Soc. *80,* 725–742.

Foxall, William (1992) Heterogeneous Slip and Rupture Models of the San Andreas Fault Zone based upon Three-Dimensional Earthquake Tomography. dissertation, University

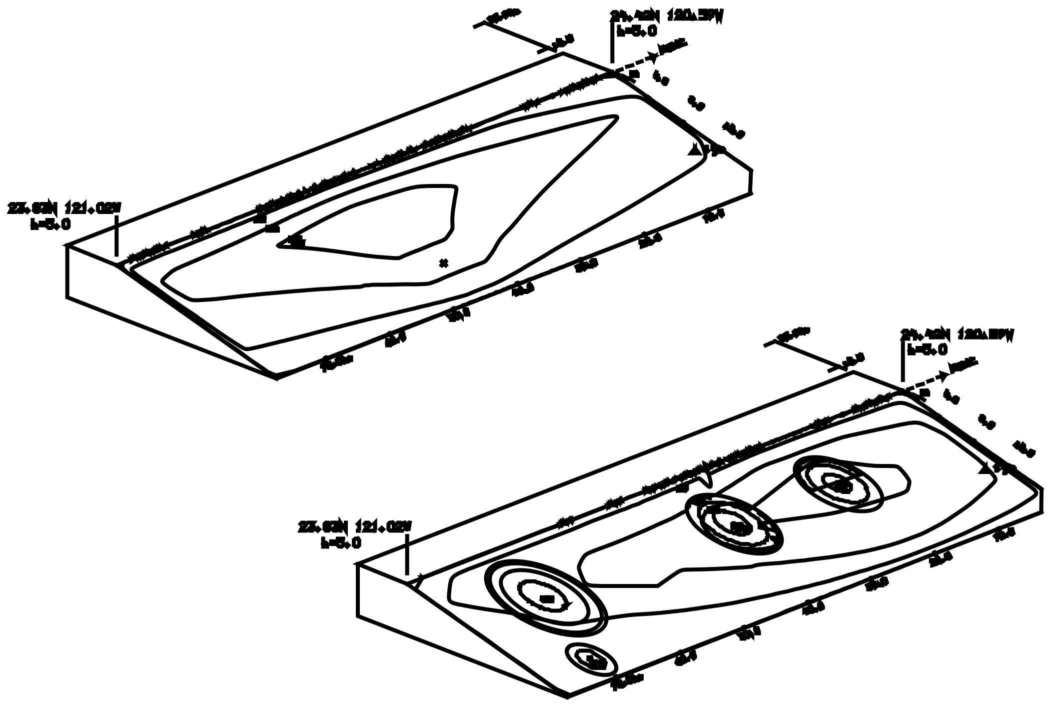

Figure 7. Slip distribution and fault geometry for models TAI01 (top) and TAI33 (bottom). The location of the hypocenter is shown by the asterisk, and the location of the site (TCU128) is shown by the triangle.

of California, Berkeley, pp.168.

Foxall, William, Lawrence Hutchings, and Paul Kasameyer (1995) Lithological and Rheological Constraints on Fault Rupture Scenarios for Ground Motion Hazard Prediction. *IUTM Symposium on Mechanics Problems in Geodynamics*, Sept. 5-9, 1994, Beijing, China; UCRL-JC 116437 Lawrence Livermore National Laboratory, pp 27. submitted to *Bul. Seis. Soc. Am.*

Frankel, Arthur (1995) Simulating strong motion of large earthquakes using recordings of small earthquakes: the Loma Prieta main shock as a test case. *Bul. Seis. Soc. Am.* **85**, pp. 1144-1160.

Freund, John E., Mathematical Statistics, 390 pp., Prentice-Hall, Englewood Cliffs, NJ., 1962.

Hadley, D.M. and D.V. Helmberger (1980). Simulation of strong ground motions. *Bul. Seis. Soc. Am.* **70**, 617-630.

Hald, A., Statistical Theory with Engineering Applications, John Wiley and Sons, New York, 1952 (1952).

Hanks, T.C. and H. Kanamori (1979) A moment magnitude scale. *J. Geophys. Res.* **84**, 2348–2350.

Hartzell, S. (1989) Comparison of seismic waveform inversion results for the rupture history of a finite fault: application to the 1986 North Palm Springs, California earthquake. *J. Geophys. Res.* **94** 7515-7534.

Hartzell, S.H. (1978). Earthquake aftershocks as Green's functions, *Geophys. Res. Lett.* **5** (1)

Hartzell, S.H. and T.H. Heaton (1988) Inversion of strong ground motion and teleseismic waveform data for the fault rupture history of the 1979 Imperial; Valley, California, earthquake. *Bul. Seis. Soc. Am.* **73**, pp. 1533-1583.

Heaton, T. H. (1982). The 1971 San Fernando earthquake: a double event? *Bul. Seis. Soc. Am.* **72**, 2037–2062.

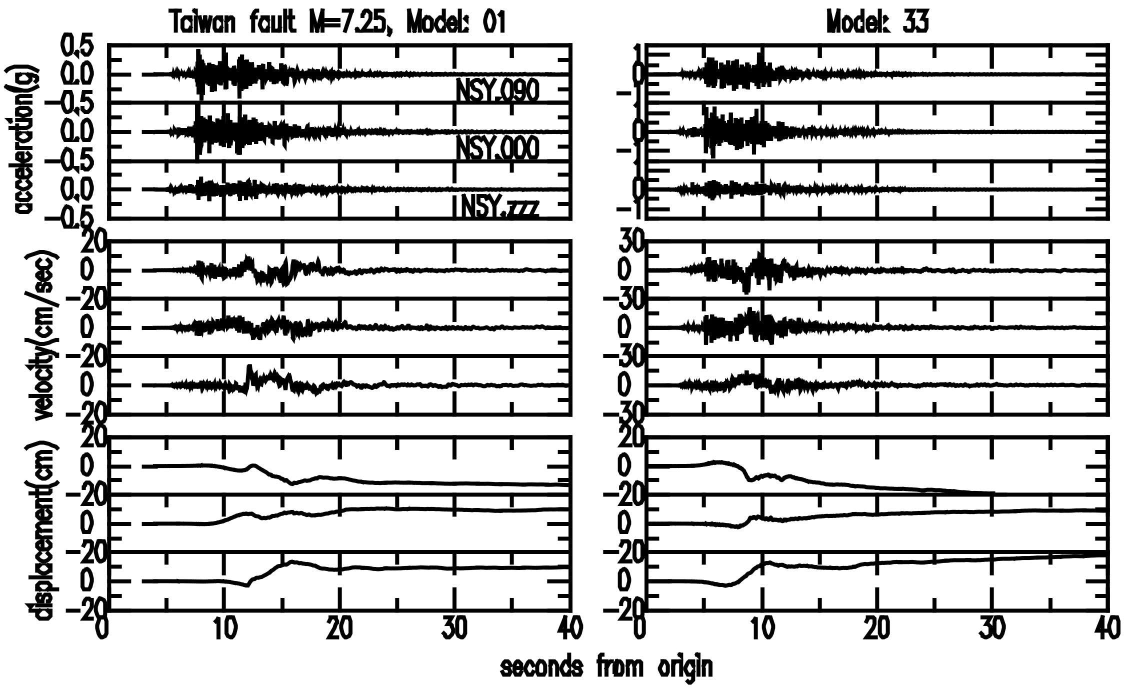

Figure 8. Acceleration (top), velocity (middle) and displacement (bottom) time histories for models TAI01 (left) and TAI33 (right).

Hsu, C.-H., C.-I Lee, and J.-F. Lee (1996) NW-SE trending seismic zone in the Miaoli-Taichung-Nantou area, central Taiwan, and its implication in tectonics, in Proceedings of the joint symposium on Taiwan Quaternary [6] and on investigation of subsurface geology and engineering environment of Taipei basin, 224-228.

Hutchings, L. (1988). Modeling strong earthquake ground motion with an earthquake simulation program EMPSYN that utilizes empirical Green's functions, Lawrence Livermore National Laboratory, Livermore, CA, *UCRL-ID-105890*, p. 122.

Hutchings, L. (1991). "Prediction" of strong ground motion for the 1989 Loma Prieta earthquake using empirical Green's functions, *Bul. Seis. Soc. Am.* **81**, 88–121.

Hutchings, L. (1994) Kinematic Earthquake Models and Synthesized Ground Motion Using Empirical Green's Functions. *Bul. Seis. Soc. Am.* **84**, pp. 1028-1050.

Hutchings, L. and F. Wu (1990). Empirical Green's functions from small earthquakes—A waveform study of locally recorded aftershocks of the San Fernando earthquake, *J. Geophys. Res*. **95**, 1187–1214.

Hutchings, L. and S. Jarpe (1996) Ground motion Variability at the Highways 14 and I-5 Interchange in the Northern San Fernando Valley. *Bul Seis Soc Am. 86,S289-S299.*

Irikura, K. (1983). Semi-empirical estimation of strong ground motions during large earthquakes. *Bull. Disaster Res. Inst*., Kyoto Univ., 33, 63-104.

Jarpe, S.P. and P.W. Kasameyer (1996). Validation of a Procedure for Calculating Broadband Strong Motion Time Histories from Empirical Green's Functions. *Bul. Seis. Soc. Am. 86, 1116-1129.*

Joyner, W. B. and D. M. Boore (1986). On simulating large earthquakes by Green's-function addition of smaller earthquakes, *Earthquake Source Mechanics*, Geophysical Monograph No. 37, Maurice Ewing, Ed., **8**, 269–274.

Kennett, B. L. N. (1983) *Seismic Wave Propagation in Stratified Media*, Cambridge University Press, Cambridge.

Kostrov, B.V. and S. Das (1988) Principles of earthquake source mechanics, in *Cam-*

bridge Monographs on Mechanics and Applied Mathematics, Cambridge University Press, Cambridge.

Lee, J.-F., T.-C. Lai, C.-H. Hsu, C.-I Lee, and K.-L. Wen, 1996. Sani-Tungshih-Puli seismic zone and their neotectonic significance, in Proceedings of the joint symposium on Taiwan Quaternary [6] and on investigation of subsurface geology and engineering environment of Taipei basin, 229-233.

McCallen, D.B. and L.J. Hutchings (1996) Ground motion estimation and nonlinear seismic analysis. Lawrence Livermore National Laboratory, Livermore, CA, UCRL-JC-121667. proceedings: 12th Conference on Analysis and Computation of the American Society of Civil Engineers, Chicago.

Munguia, L. and J. Brune (1984). Simulation of strong ground motion for earthquakes in the Mexicali-Imperial Valley region, *Geophys. J. Royal Astr. Soc.* **79**, 747–771.

Papageorgiou, A.S. and K. Aki (1983). A specific Barrier model for the Quantitative description of inhomogeneous faulting and the prediction of strong ground motion. I. Description of the model. *Bul. Seis. Soc. Am.* **73**, 693–722.

Rice, J.R. and A.L. Ruina (1983) Stability of steady friction slipping. *J. Appl. Mech.*, **105**, 343-349.

Rau, Ruey-Juin and Francis T. Wu (1995) Tomographic imaging of lithospheric structures under Taiwan, Earth Planet. Sci. Lett., **133**, pp 517-532.

Wald, D.J., D.V. Helmberger and S.H. Hartzell (1990) Rupture process of the 1987 Superstition Hills Earthquake from inversion of Strong-Motion Data. *Bul. Seis. Soc. Am.* **80**, 1079–1098.

Wald, David J., Hiroo Kanamori, Donald V. Helmberger, and Thomas Heaton (1993) Source Study of the 1906 San Francisco Earthquake. *Bul. Seis. Soc. Am.* **83**, pp. 981-1019.

Wald, David J., Donald V. Helmberger, and Thomas H. Heaton (1991) Rupture Model of the 1989 Loma Prieta Earthquake from Inversion of Strong-Motion and Broadband Teleseismic Data. *Bul. Seis. Soc. Am.* **81**, 1540–1572.

Wald, D. J., T. H. Heaton, and K.W. Hudnut (1995) The Slip History of the 1994 Northridge, California Earthquake Determined from Strong -Motion, Teleseismic, GPS, and Leveling Data. preprint, *Bul. Seism. Soc. Am.* **81** (1).

Wennerberg, L. (1990). Stochastic summation of empirical Green's functions, *Bul. Seis. Soc. Am.* **80**, 1418–1432.

Wu, F. T. (1978). Prediction of Strong Ground Motion using Small Earthquakes, *Proc. 2nd International Microzonation Conference* **2**, 701–704.

Wu, Francis T., Ruey-Juin Rau, and David Salzberg (1996) Taiwan Orogeny: Thin-Skinned or Lithospheric Collision? preprint, *Tectonophysics*.

Scholz, C.H. (1990) *The mechanics of Earthquake Faulting*, Cambridge University Press, Cambridge, 439p.

Tumarkin, A.G., R.J. Archuleta, and R. Madariaga (1994) Basic scaling relations for composite models, *Bull. Seism. Soc. Am.* **84**, no 4.